Sub-kHz-linewidth external-cavity laser (ECL) with Si₃N₄ resonator used as a tunable pump for a Kerr frequency comb

Pascal Maier,[1,2,*] Yung Chen,[1] Yilin Xu,[1,2] Yiyang Bao,[1,2] Matthias Blaicher,[1,2] Dimitri Geskus,[3] Ronald Dekker,[3] Junqiu Liu,[4] Philipp-Immanuel Dietrich,[1,2,5] Huanfa Peng,[1] Sebastian Randel,[1] Wolfgang Freude,[1] Tobias J. Kippenberg,[4,6] and Christian Koos[1,2,5,6,*]

[1]*Institute of Photonics and Quantum Electronics (IPQ), Karlsruhe Institute of Technology (KIT), Engesserstr. 5, 76131 Karlsruhe, Germany*
[2]*Institute of Microstructure Technology (IMT), Karlsruhe Institute of Technology (KIT), Hermann-von-Helmholtz-Platz 1, 76344 Eggenstein-Leopoldshafen, Germany*
[3]*LioniX International B.V., P.O. Box 456, 7500 AL Enschede, The Netherlands*
[4]*École Polytechnique Fédérale de Lausanne (EPFL), Rte Cantonale, 1015 Lausanne, Switzerland*
[5]*Vanguard Automation GmbH, Gablonzer Str. 10, 76185 Karlsruhe, Germany*
[6]*Deeplight S.A., Fondation EPFL Innovation Park – Bâtiment C, 1015 Lausanne, Switzerland*
* pascal.maier@kit.edu; christian.koos@kit.edu

Abstract: Combining optical gain in direct-bandgap III-V materials with tunable optical feedback offered by advanced photonic integrated circuits is key to chip-scale external-cavity lasers (ECL), offering wideband tunability along with low optical linewidths. External feedback circuits can be efficiently implemented using low-loss silicon nitride (Si₃N₄) waveguides, which do not suffer from two-photon absorption and can thus handle much higher power levels than conventional silicon photonics. However, co-integrating III-V-based gain elements with tunable external feedback circuits in chip-scale modules still represents a challenge, requiring either technologically demanding heterogeneous integration techniques or costly high-precision multi-chip assembly, often based on active alignment. In this work, we demonstrate Si₃N₄-based hybrid integrated ECL that exploit 3D-printed structures such as intra-cavity photonic wire bonds and facet-attached microlenses for low-loss optical coupling with relaxed alignment tolerances, thereby overcoming the need for active alignment while maintaining the full flexibility of multi-chip integration techniques. In a proof-of-concept experiment, we demonstrate an ECL offering a 90 nm tuning range (1480 nm–1570 nm) with a side-mode suppression ratio of typically 60 dB along with on-chip output powers above 12 dBm. We measure an intrinsic linewidth of 979 Hz, which is among the lowest values reported for comparable feedback architectures. The optical loss of the intra-cavity photonic wire bond between the III-V gain element and the Si₃N₄-based tunable feedback circuit amounts to approximately $(1.6 \pm 0.2)\,\text{dB}$. We use the ECL as a tunable pump laser to generate a dissipative Kerr soliton frequency comb. To the best of our knowledge, our experiments represent the first demonstration of a single-soliton Kerr comb generated with a pump that is derived from a hybrid ECL.

1. Introduction

Tunable lasers are key building blocks of integrated optics. In this context, hybrid external-cavity lasers (ECL) are particularly interesting, opening the possibility to combine optical amplification in direct-bandgap III-V-based gain elements with tunable optical feedback offered by advanced passive photonic integrated circuits (PIC). Such feedback circuits can be efficiently implemented on the silicon photonic (SiP) platform [1–8]. Alternatively, silicon nitride (Si₃N₄) waveguides can be used for the feedback circuits [9–16], offering much lower linear and nonlinear losses than their SiP counterparts. This increases the intrinsic Q-factors of resonator-based feedback circuits and eliminates two-photon absorption (TPA) as a critical impairment at high power levels, thereby permitting greatly reduced phase noise and small linewidths [9,17,18]. However, the co-integration of III-V-based gain elements and tunable external-cavity circuits in chip-scale packages still represents a challenge. Specifically, heterogeneous integration based on transfer of InGaAsP epitaxial layers to pre-processed passive silicon or silicon nitride PIC paves a path towards high-density monolithic integration, but the underlying processes are still complex [19] and mostly limited to the SiP platform. This approach is hence mainly suited for high-volume applications that justify the associated technological overhead. Alternatively, III-V-dies and passive feedback circuits can first be processed on separate substrates and then be combined in a compact multi-chip module using a hybrid approach. This concept allows the components to be optimized and tested individually and facilitates thermal decoupling of the gain element from temperature-sensitive feedback circuits. However, assembly of hybrid photonic multi-chip modules crucially relies on high-precision alignment of the underlying optical dies, often requiring active alignment techniques, where the

coupling efficiency is continuously measured and optimized during the assembly process [2,8–12,14–16]. This leads to limited fabrication throughput and often hinders cost-efficient scalability to high volumes.

In this paper, we demonstrate Si_3N_4-based hybrid integrated ECL that exploit photonic wire bonds (PWB) as intra-cavity coupling elements between reflective semiconductor optical amplifiers (RSOA) and the associated external-cavity circuits [20]. PWB are structured *in-situ* in a fully automated process with shapes adapted to the mode-field sizes and the positions of the chips at both ends, thus offering low coupling loss even for vastly dissimilar waveguide cross sections and limited placement accuracy of the underlying dies [21]. In a proof-of-concept experiment, we demonstrate an ECL offering a 90 nm tuning range (1480 nm–1570 nm) with a side-mode suppression ratio of typically 60 dB along with on-chip output powers above 12 dBm. We measure an intrinsic linewidth of 979 Hz, which is among the lowest values reported for comparable feedback architectures. The optical loss of the intra-cavity PWB between the III-V gain element and the Si_3N_4-based tunable feedback circuit amounts to approximately $(1.6 \pm 0.2)\,dB$. At the output, the Si_3N_4-based tunable feedback circuit is coupled to an array of single-mode fibers using 3D-printed facet-attached microlenses (FaML) [22–24]. To demonstrate the performance and the versatility of the device, we use the ECL as narrow-linewidth tunable pump laser for generation of dissipative Kerr soliton (DKS) frequency combs in high-Q Si_3N_4 microresonators. To the best of our knowledge, our experiments represent the first demonstration of a single-soliton Kerr comb generated with a pump that is derived from a hybrid integrated ECL.

2. Integrated hybrid external-cavity laser (ECL)
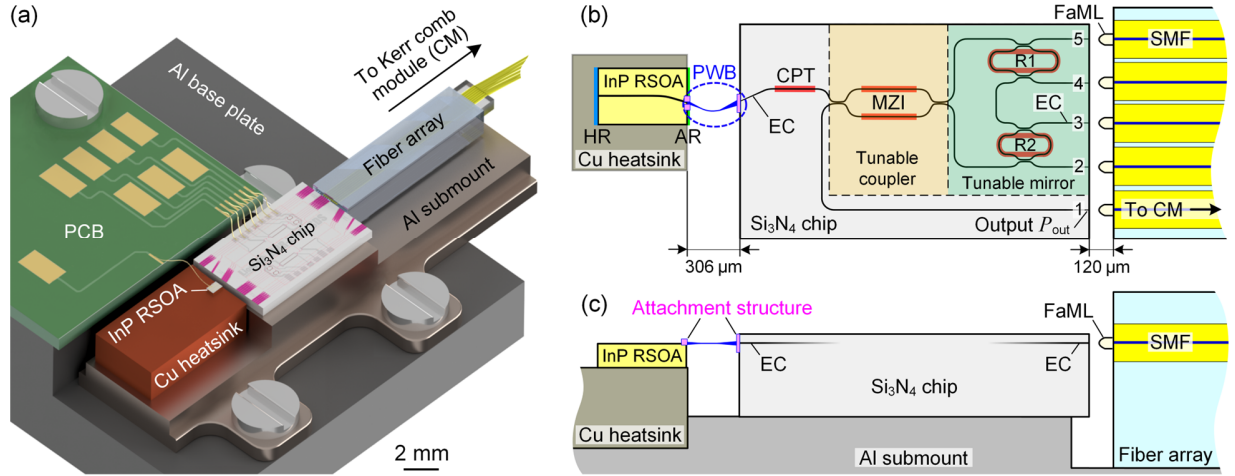
2.1 Device concept

The concept of a hybrid integrated ECL with 3D-printed intra-cavity photonic wire bond (PWB) and facet-attached microlenses (FaML) is shown in Fig. 1(a). The assembly consists of two dies on a common aluminum (Al) submount – an InP reflective semiconductor optical amplifier (RSOA) attached to a copper (Cu) heatsink and a Si_3N_4-based external-cavity circuit with a fiber array at the output. The device is controlled via an electronic circuit on a printed circuit board (PCB), which is attached to an Al base plate together with the submount. Figure 1(b) provides a top-view schematic of the InP RSOA and the Si_3N_4 chip, the latter comprising a Sagnac loop mirror with a Vernier pair of tunable racetrack resonators R1 and R2, a cavity phase tuner (CPT), and a tunable output coupler implemented as a Mach-Zehnder interferometer (MZI). The RSOA has a back facet with a high-reflectivity (HR) coating, while the front facet is angled at 9.0° and has an anti-reflection (AR) coating with respect to polymer. A PWB bridges the gap between the RSOA front facet and the edge coupler (EC) on the Si_3N_4 chip. This EC consists of a tapered waveguide (WG) which is oriented at an angle of 19.9° with respect to the facet normal. A side-view schematic of the module is provided in Fig. 1(c). Each end of the PWB is equipped with additional attachment structures that improve mechanical stability. Note that the PWB approach allows for connecting the two dies even though the emission angle of the RSOA output and the direction of the input EC of the Si_3N_4 chip are not matched, emphasizing the flexibility of the concept. The Si_3N_4 racetrack resonators, MZI, and CPT are tuned by thermal phase shifters. The CPT is used to adjust the cavity round-trip phase to an integer multiple of 2π at the wavelength corresponding to the maximum mirror reflectivity. The tunable MZI-based output coupler is used to set the ratio between the light extracted from the laser cavity and the feedback to the RSOA.

In the device implementation discussed in the following, the CPT is 1 mm long, and the Vernier pair of racetrack resonators have perimeters of 885.1 μm (R1) and 857.4 μm (R2). Four auxiliary waveguides WG 2…5 and the output WG 1 are routed to the Si_3N_4 chip edge and connected to tapered EC having a pitch of 127 μm. All five waveguide ports 1…5 are coupled to a single-mode fiber (SMF) array (FA) via 3D-printed FaML.

2.2 Device concept

To fully evaluate our integration concept, all components of the ECL are individually characterized prior to assembly. The assembly of fully characterized known-good components highlights one of the key advantages of our hybrid approach compared to other integration concepts. The following sections describe the measured performance of the RSOA and of the Si_3N_4 feedback circuit.

The C-band RSOA (Fraunhofer Heinrich-Hertz-Institut, Germany) is 700 μm long, has a back facet with a HR coating (90% reflectivity with respect to air) and an angled front facet (9°) with AR coating designed for emission into polymer ($n = 1.56$). The device is similar to the RSOA used in [1], and further details relating to the measurement techniques are described in the associated Supplementary Information. At a pump current of 100 mA, the measured maximum small-signal gain is 22 dB, and the saturated output power is $P_{sat} = 11.4\,dBm$, both obtained at a wavelength of $\lambda = 1550\,nm$. The RSOA characterization results are given in more detail in the Appendix, see Fig. 4(a) and the associated description.

Fig. 1. Concept of a hybrid integrated ECL module with a 3D-printed intra-cavity photonic wire bond (PWB) and facet-attached microlenses (FaML). **(a)** The ECL assembly consists of two dies on a common aluminum (Al) submount – an InP reflective semiconductor optical amplifier (RSOA) attached to a copper (Cu) heatsink and a Si_3N_4-based external-cavity circuit with a fiber array at the output. The device is controlled via an electronic circuit on a printed circuit board (PCB), which is attached to an Al base plate together with the submount. The fiber-coupled ECL output can be connected to the Kerr comb module (CM), see Fig. 3(a). **(b)** Top-view schematic of the InP RSOA and the Si_3N_4 chip, the latter comprising a Sagnac loop mirror with a Vernier pair of tunable racetrack resonators R1 and R2, a cavity phase tuner (CPT), and a tunable output coupler implemented as a Mach-Zehnder interferometer (MZI). The RSOA has a back facet with a high-reflectivity (HR) coating, while the front facet is angled at 9.0° and has an anti-reflection (AR) coating with respect to polymer. The intra-cavity PWB bridges the gap of 306 µm between the RSOA front facet and the edge coupler (EC) on the Si_3N_4 chip. This EC consists of a tapered waveguide (WG), which is oriented at an angle of 19.9° with respect to the facet normal. Note that the PWB approach allows for connecting the two dies even though the emission direction of the on-chip waveguides at its ends are not matched, emphasizing the flexibility of the concept. In our device implementation, the CPT is 1 mm long and the Vernier pair of racetrack resonators have perimeters of 885.1 µm (R1) and 857.4 µm (R2). Four auxiliary waveguides WG 2…5 and the output WG 1 are routed to the Si_3N_4 chip edge and connected to associated tapered EC having a pitch of 127 µm. All five waveguide ports 1…5 are coupled to a single-mode fiber (SMF) array via 3D-printed FaML. **(c)** Side-view schematic of the module. Each end of the PWB is equipped with additional attachment structures that improve mechanical stability. A step on the Al submount is used to align the height of the RSOA chip surface to that of the WG layer containing the EC on the Si_3N_4 side.

Frequency-selective optical feedback is provided by a Vernier pair of racetrack resonators on the Si_3N_4 chip (TriPleX®, LioniX International B.V., The Netherlands), Fig. 1(b). Both racetrack resonators have equal WG cross sections, therefore identical propagation constants, and slightly different free spectral ranges (FSR) due to slight differences of the perimeters. The individual racetrack resonators are characterized by power transmission measurements in a loop-back configuration through the two auxiliary waveguide ports 3 and 4, see Fig. 1(b). The measured transmission can be fit to a model [1] to estimate the resonator parameters such as the loaded Q-factors and the FSR. At a wavelength of 1550 nm, we extract FSR of 198.5 GHz and 204.8 GHz for R1 and R2, respectively, along with approximately equal loaded Q-factors of 20 000. With these numbers, we can calculate a 0.1 dB on-chip reflection loss of the tunable mirror, measured at the top of the reflection peak in case a resonance of R1 coincides perfectly with a corresponding resonance of R2.

2.3 Module assembly

In a first step of module assembly, the RSOA is glued to a copper (Cu) heatsink with an electrically conductive adhesive (EPO-TEK® H20E, Epoxy Technology Inc., USA). The Cu heatsink with the RSOA and the Si_3N_4 chip are then coarsely aligned to each other and glued to an Al submount, see Fig. 1(a). A step on the Al submount is used to align the height of the RSOA chip surface to that of the WG layer containing the EC on the Si_3N_4 side. The PWB trajectory depends on the exact positions and emission directions of the RSOA and Si_3N_4 EC facets, see Fig. 1(b). In our implementation, the PWB bridges a gap of 306 µm between the two dies. The PWB on the RSOA side comprises a taper with an initial cross-section of 4.0 µm × 4.0 µm, matched to the mode-field size at the RSOA facet. The PWB cross-section is then reduced to the usual 2.4 µm × 2.0 µm. At the facet of the Si_3N_4 chip, the PWB is up-tapered to a final cross-section of 8.0 µm × 5.0 µm connecting to the on-chip Si_3N_4 EC. Between the tapers, the PWB maintains the constant cross-section of 2.4 µm × 2.0 µm, while the trajectory describes an arc to smoothly connect to the edge-coupled on-chip WG at either end, which feature notably different directions. Printed attachment structures on both the RSOA and the Si_3N_4 chip facets improve the mechanical stability of the PWB, see Fig. 1(c). Fiber-chip coupling at the output of the Si_3N_4 chip relies on five identical FaML, printed to the facets of the FA. The FaML are 70 µm long and have been designed for a working distance of 50 µm between the apices of the lenses and the Si_3N_4 WG facets. The distance between the FA and the Si_3N_4 chip facet hence amounts to 120 µm, see Fig. 1(b).
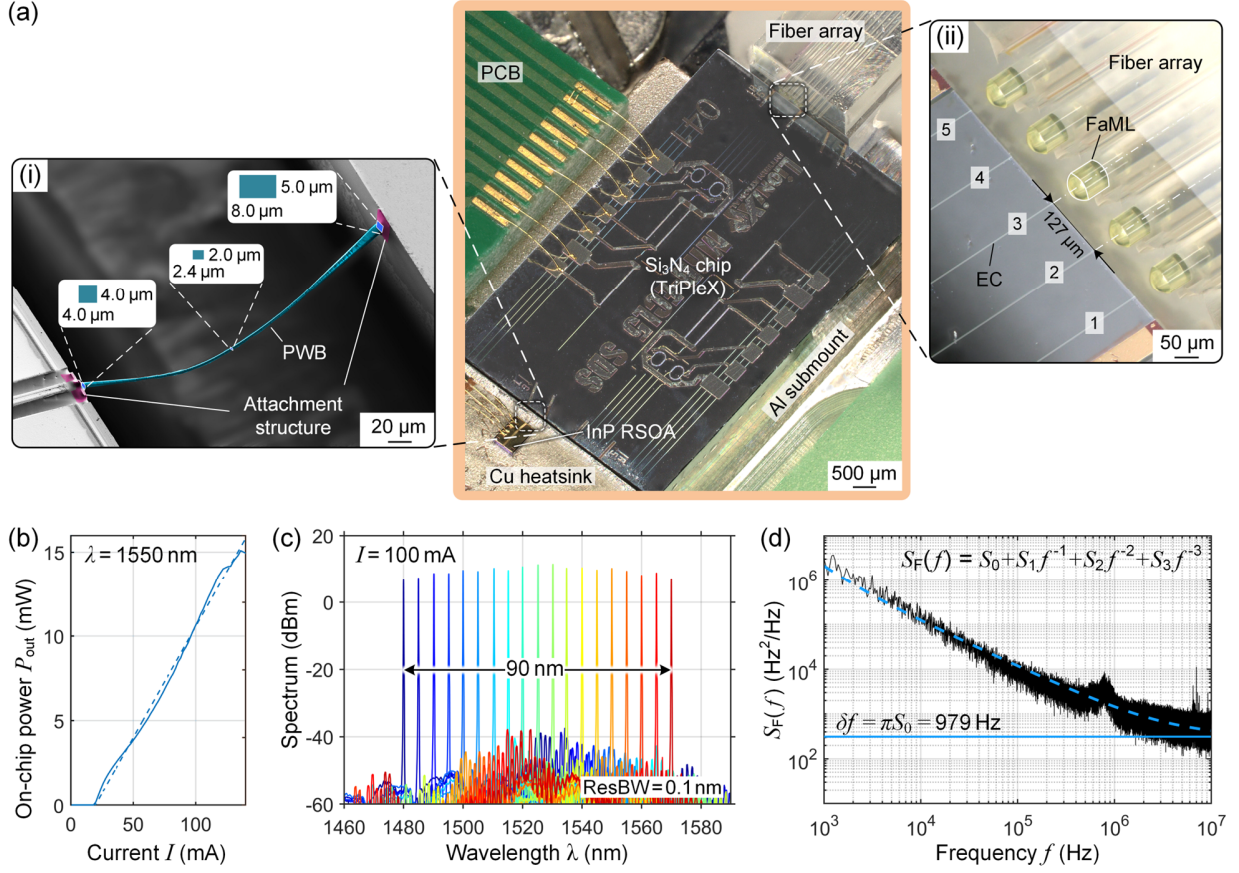
Fig. 2. Implementation of ECL module and performance characterization. **(a)** Microscope image of the assembled ECL module according to Fig. 1(a). Inset (i) shows a scanning-electron microscope (SEM) image of the false-colored PWB between the RSOA and Si_3N_4 (TriPleX®) chip. The various cross-sections at different positions along the PWB are marked. Inset (ii) displays a microscope image of the five FaML on the FA having a pitch of $127\,\mu m$ and facing the corresponding EC of the waveguide ports 1…5 on the Si_3N_4 chip. **(b)** On-chip output power P_{out} vs. injection current I for lasing at 1550 nm, leading to a threshold current of 19 mA and an average slope efficiency of 132 mW/A (fit by dashed straight line). **(c)** Superimposed ECL lasing spectra with tuning steps of 5 nm within the tuning range $(1480…1570)\,nm$ for $I = 100\,mA$. The maximum on-chip output power is 12 dBm near a wavelength of 1525 nm. The side-mode suppression ratio (SMSR) is > 50 dB and can reach 60 dB when avoiding the borders of the tuning range. **(d)** FM noise spectrum with fit (blue dashed line). The intrinsic (Lorentzian) linewidth is $\delta f = \pi S_0 = 979\,Hz$ (fit by solid blue line).

Both the PWB and the FaML are made from a negative-tone photoresist (VanCoreA, Vanguard Automation GmbH, Germany; refractive index $n = 1.53$) by *in-situ* multi-photon lithography. The fabricated PWB and FaML are developed in propylene-glycol-methyl-etheracetate (PGMEA), flushed with isopropanol, and finally blow-dried. The FaML on the FA are 3D-printed in a separate step for subsequent assembly with a custom pick-and-place machine [24]. Figure 2(a) shows a microscope image of the fully assembled ECL module. Inset (i) displays a scanning-electron microscope (SEM) image of the false-colored PWB along with the dimensions of the various PWB cross-sections. Inset (ii) shows a microscope image of the five FaML on the FA facing the corresponding edge-coupled waveguide ports 1…5 on the Si_3N_4 chip.

2.4 Module characterization

The ECL wavelength is selected by aligning the two racetrack resonators to a common resonance, which may be detected through the two auxiliary waveguide ports 3 and 4 in a loop-back configuration. After the alignment of the resonances, the cavity phase and the tunable coupler are adjusted for maximum on-chip output power P_{out}, see Fig. 1(b). From the power-current characteristics (*P-I*-curve) in Fig. 2(b) measured at a wavelength $\lambda = 1550\,nm$, we extract a threshold current of 19 mA and an average slope efficiency of 132 mW/A. We further estimate a PWB loss of $(1.6 \pm 0.2)\,dB$ by measuring the ECL emission power P_{out} and by comparing it to the measured saturated output power P_{sat} of the RSOA at the same wavelength $\lambda = 1550\,nm$ and at the same injection current I. Details relating to the estimation of the PWB losses can be found in the Appendix. The measured PWB loss is on par with previously reported coupling losses of $(1.6 \pm 1.0)\,dB$ between RSOA and Si_3N_4-based PIC using passive alignment [25],

4

outperforming many previous demonstrations featuring typical RSOA-to-chip insertion losses of (2…3) dB [11,13,15,16,26]. Butt-coupling losses below 1 dB are also feasible, but the associated devices require carefully laid-out spot size converters (SSC) on the passive chips [2,3] or inverse tapers on both the active and passive chips [7,27], usually in conjunction with active alignment techniques for precise positioning.

Figure 2(c) depicts superimposed ECL lasing spectra with tuning steps of 5 nm within the tuning range (1480…1570) nm for a fixed injection current of $I = 100$ mA. A maximum on-chip output power P_{out} of 12 dBm is measured at wavelengths near 1525 nm, close to the center wavelength of the RSOA gain spectrum. The SMSR is larger than 50 dB over the whole tuning range and amounts to typically 60 dB when avoiding the borders of the tuning range.

We further measure the phase noise of the emitted laser line using a frequency discriminator (LWA-1k 1550, HighFinesse GmbH, Germany). The measurements are carried out for an emission wavelength close to 1550 nm, where we re-adjust the tunable output coupler for minimum intrinsic linewidth. The associated FM noise spectrum is shown in Fig. 2(d). The intrinsic (Lorentzian) linewidth is obtained by first fitting a model function of the form $S_F(f) = S_0 + S_1 f^{-1} + S_2 f^{-2} + S_3 f^{-3}$ to the measured FM noise spectrum (blue dashed line). This leads to $S_0 = 311 \text{Hz}^2/\text{Hz}$, corresponding to an intrinsic linewidth of $\delta f = \pi S_0 = 979$ Hz (solid blue line), which is among the lowest values reported for similar feedback architectures [2–4,6,9–12]. The low phase noise results from the large effective optical cavity length (48.3 mm), the low passive WG losses (0.1 dB/cm), and the small RSOA-to-chip coupling loss (1.6 dB). Minimizing losses in the extended laser cavity, which are dictated mainly by the RSOA-to-chip coupling loss, is essential to obtain low laser linewidths [26]. Our results are on par with lately demonstrated linewidths of 895 Hz [12], achieved with actively aligned Si_3N_4-based external cavity circuits featuring only a pair of Vernier-type ring resonators. Note that previously reported demonstrations of such devices usually reached values of the order of 2 kHz [9,10]. Lower intrinsic linewidths may be achieved by using external cavity circuits with three or more ring resonators: Using shallow-etched low-loss SiP rib WG in combination with three-ring external cavity circuits, heterogeneously integrated ECL with linewidths down to 95 Hz have been demonstrated [5]. The linewidths of three-ring ECL can be further reduced down to 40 Hz by using Si_3N_4-based external cavity circuits with large optical cavity lengths of the order of 0.5 m [14]. Note that feedback circuits based on standard SiP strip WG generally lead to larger intrinsic linewidths of, e.g., 12 kHz, demonstrated with a hybrid integrated ECL based on a pair of Vernier-type SiP ring resonators in combination with a Mach-Zehnder-type delay interferometer that additionally suppresses Vernier side-lobes in the filter transfer function [8].

3. Kerr comb generation

To demonstrate the versatility of our hybrid ECL, we use the device as a precisely tunable pump laser to generate dissipative Kerr soliton (DKS) frequency combs in Si_3N_4 microresonators. Figure 3(a) shows a schematic of the associated experimental setup: The ECL fiber output is connected to an optical isolator, followed by an erbium-doped fiber amplifier (EDFA) and a polarization controller (PC). The light is then fed via a PWB to a separately packaged comb module (CM), consisting of a ring resonator (R3, diameter 1286 μm, free spectral range 35.4 GHz, $Q \approx 15 \times 10^6$), which was fabricated using the photonic Damascene process [28]. A microscope image of the CM is shown at the bottom of Fig. 3(a) along with a top-view schematic of the Si_3N_4 chip. Besides the ring resonator R3 of interest, the chip contains two additional rings that were not used in our experiments. The output of the ring resonator R3 is connected to a subsequent FA by a PWB. The input and output FA as well as the Si_3N_4 chip are fixed to a common Al submount.

The start-up process for the comb source is illustrated in Fig. 3(b) [29,30]. The left axis indicates the absolute wavelength of the ECL, whereas the axis on the right shows the associated detuning $f_{ECL} - f_{R3,cold}$ of the ECL frequency f_{ECL} with respect to the cold resonance of R3 $f_{R3,cold} = 193.5348$ THz (horizontal green line). Initially, the ECL wavelength (♦, I) is blue-detuned with respect to the cold resonance of R3. Then the ECL emission wavelength is increased by ramping up the CPT heater power, see black dots in Fig. 3(b) and Arrow ①. Upon reaching the red-detuned regime, $f_{ECL} < f_{R3,cold}$, a multi-soliton state can be observed (♦, II). Subsequently, the ECL pump is tuned backwards [29,30] (Arrow ②), thereby reducing the number of solitons circulating in the cavity (♦, III), until finally, a single-soliton state is reached at an ECL wavelength slightly above the cold resonance of R3 (♦, IV). For the states (♦, III) and (♦, IV), we record the spectrum using an optical spectrum analyzer (OSA), Fig. 3(c) and Fig. 3(d). The spectral envelope of the single-soliton state (♦, IV) is smooth and can be well approximated by the typical sech^2-characteristic, Fig. 3(d), whereas the multi-soliton state (♦, III) is characterized by spectral fringes, Fig. 3(c). To the best of our knowledge, our experiments represent the first demonstration of a single-soliton Kerr comb generated with a pump that is derived from a hybrid integrated ECL.
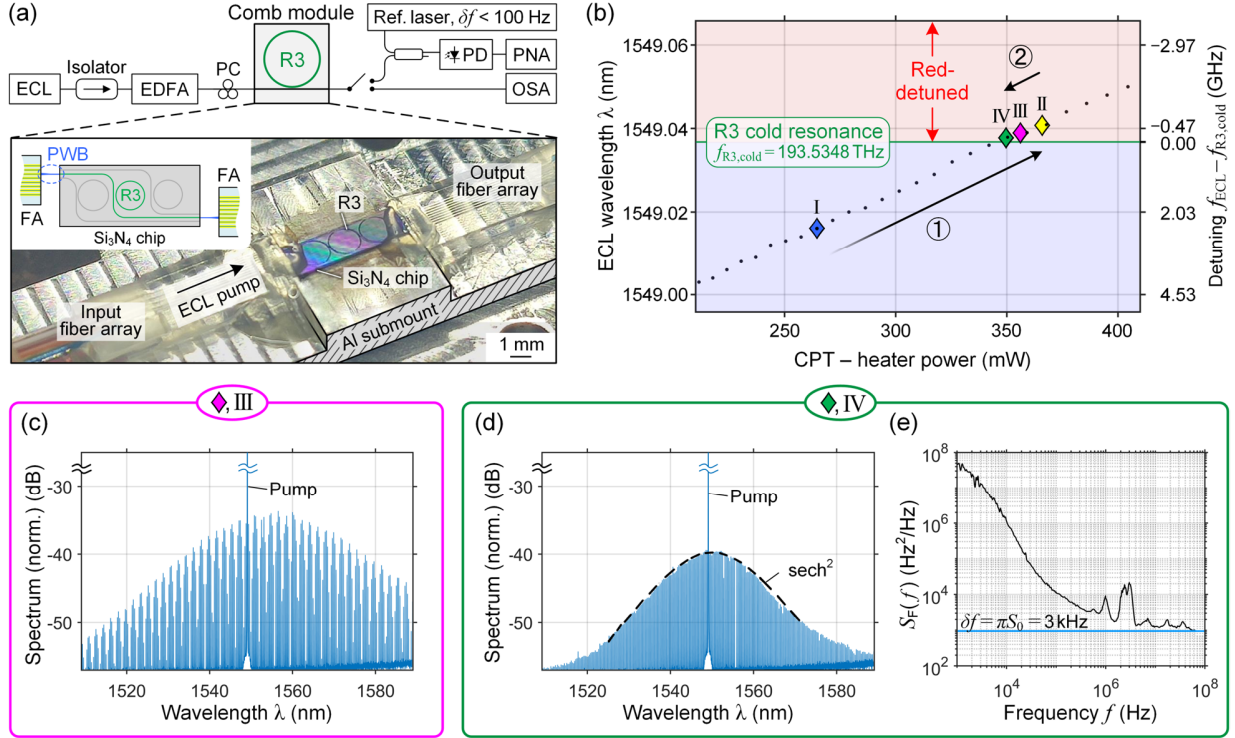
Fig. 3. Dissipative Kerr soliton (DKS) frequency comb generation in a high-Q Si_3N_4 microresonator (R3) using the ECL module as a precisely tunable pump laser. **(a)** Schematic of the associated experimental setup: The ECL fiber output is connected to an optical isolator followed by an erbium-doped fiber amplifier (EDFA) and a polarization controller (PC). The light is then fed via a PWB to a separately packaged comb module (CM), consisting of a ring resonator (R3, diameter 1286 µm, free spectral range 35.4 GHz, $Q \approx 15 \times 10^6$), which was fabricated using the photonic Damascene process. A microscope image of the CM is shown in the bottom part of the figure along with a top-view schematic of the Si_3N_4 chip. Besides the ring resonator R3 of interest, the chip contains two additional rings that were not used in our experiments. The output of the ring resonator R3 is connected to a subsequent FA by a second PWB. The input and output FA as well as the Si_3N_4 chip are fixed to a common Al submount. The output of the CM is either monitored on an optical spectrum analyzer (OSA) or beat with a highly stable reference laser tone. The photocurrent at the intermediate frequency is sent to a phase-noise analyzer (PNA). **(b)** Start-up process for the comb source, relying on precise tuning of the ECL emission wavelength. The left axis indicates the absolute wavelength of the ECL, whereas the axis on the right shows the associated detuning $f_{ECL} - f_{R3,cold}$ of the ECL frequency f_{ECL} with respect to the cold resonance of R3 $f_{R3,cold} = 193.5348\,THz$ (horizontal green line). Initially, the ECL wavelength ($\blacklozenge$, I) is blue-detuned with respect to the cold resonance of R3. Then the ECL emission wavelength is increased by ramping up the CPT heater power, see black dots in Fig. 3(b) and Arrow ①. Upon reaching the red-detuned regime, $f_{ECL} < f_{R3,cold}$, a multi-soliton state can be observed ($\blacklozenge$, II). Subsequently, the ECL pump is tuned backwards (Arrow ②), thereby reducing the number of solitons circulating in the cavity ($\blacklozenge$, III), until finally, a single-soliton state is reached at an ECL wavelength slightly above the cold resonance of R3 ($\blacklozenge$, IV). **(c)** Spectrum of an exemplary multi-soliton comb, characterized by spectral fringes. The multi-soliton state is indicated by a pink diamond ($\blacklozenge$, III) in (b). **(d)** Spectrum of single-soliton comb, characterized by a smooth spectral envelope, which can be well approximated by the typical $sech^2$-characteristic. The single-soliton state is indicated by a green diamond ($\blacklozenge$, IV) in (b). **(e)** FM noise spectrum of a typical single-soliton comb line. We estimate an intrinsic linewidth of $\delta f = 3\,kHz$.

We also measure the FM noise spectrum of a typical single-soliton comb line, Fig. 3(e), by beating it with a highly stable reference laser tone (Koheras X15, NKT Photonics A/S, Denmark; intrinsic linewidth $\delta f < 100\,Hz$) on a photodetector (PD). The photocurrent at the intermediate frequency is sent to a phase-noise analyzer (PNA, FSWP50, Rohde & Schwarz GmbH & Co. KG, Germany). From the recorded FM noise spectrum, an intrinsic linewidth of $\delta f = 3\,kHz$ is estimated, dictated by the phase noise of the ECL. Note that the operating point of the ECL was not optimized for minimum phase noise and that the linewidth was therefore slightly higher than the one shown in Fig. 2(d). Note also that the Kerr comb generator used here features a threshold pump power of the order of $(10...15)\,mW$ [31,32], which may be reduced further to below 5 mW [16], e.g., by increasing the quality factor of the ring resonator [16,33]. Leveraging the full 15 mW of on-chip ECL power by co-integrating the Si_3N_4 microresonators with the external feedback circuit of the ECL would allow to omit the EDFA and to build a fully integrated Kerr comb module similar to the one demonstrated in [16]. Note that pumping a Kerr comb generator by a freely tunable continuous-wave (CW) laser allows to independently control the detuning of the pump tone from the resonance of the cold ring, which is impossible for Kerr comb generators that are based on self-injection locking (SIL) of the pump laser to the Kerr-nonlinear resonator [16,33–38]. This additional degree of freedom allows to optimize the generated frequency comb, e.g., with respect to bandwidth or comb-line power [35].

4. Summary

We demonstrate a hybrid integrated ECL that exploits an intra-cavity photonic wire bond (PWB) for connecting an InP reflective semiconductor optical amplifier (RSOA) to a Si$_3$N$_4$-based tunable external-cavity circuit. Photonic wire bonding overcomes the need for high-precision alignment during assembly, thereby permitting fully automated mass production of hybrid photonic multi-chip assemblies. The ECL features a tuning range of 90 nm between 1480 nm and 1570 nm, a maximum on-chip output power of 12 dBm, and a typical side-mode suppression ratio larger than 60 dB. Upon optimization of the operating point, we measure an intrinsic linewidth of 979 Hz, which is among the lowest values reported for two-ring feedback architectures. The versatility of the ECL is demonstrated by using the device as narrow-linewidth tunable pump laser for Kerr frequency comb generation in a high-Q Si$_3$N$_4$ microresonator. To the best of our knowledge, our experiments represent the first demonstration of a single-soliton Kerr comb generated with a pump that is derived from a hybrid integrated ECL. We believe that our experiments pave a path towards highly versatile hybrid light sources that combine the scalability advantages of monolithic integration with the performance and flexibility of hybrid multi-chip assemblies.
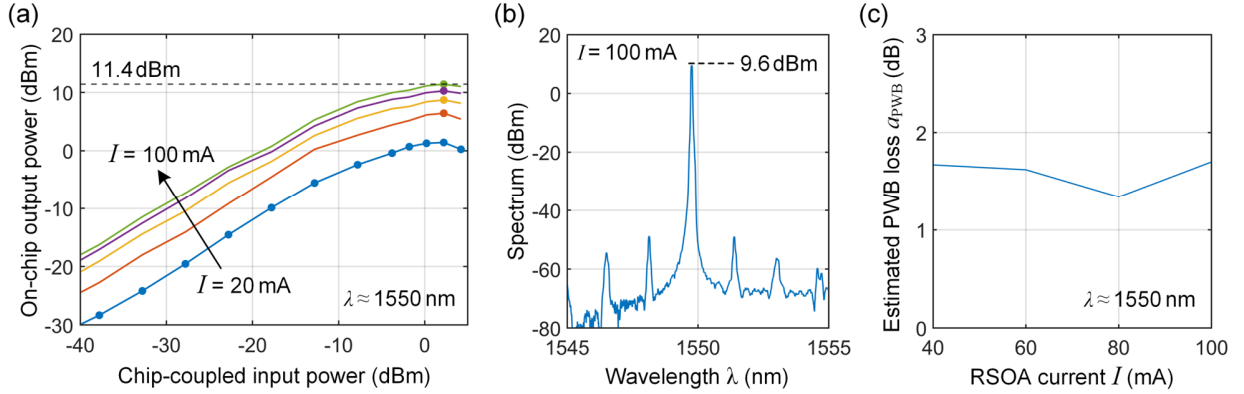
Appendix

Photonic wire bond loss estimation

For estimating the PWB loss, we compare the on-chip output power P_{out} of the ECL to the saturated output power P_{sat} of the RSOA at the same wavelength λ and at the same injection currents I. As a first step, we use the data obtained from the RSOA characterization prior to assembly of the ECL module and extract the current-dependent saturated RSOA output power $P_{sat}(I)$. To this end, we launch light at a wavelength $\lambda \approx 1550\,\text{nm}$ into the RSOA through a circulator using an AR-coated lensed single-mode fiber (SMF) and measure the amplified signal after the circulator. The RSOA is similar to the one used in [1], where the details of the measurement technique are described in the Supplementary Information. In our measurements, we vary the RSOA pump current between 20 mA and 100 mA in steps of 20 mA and derive the associated relationships between the RSOA input and output power, both measured at the RSOA chip facet, see Fig. 4(a). The device was tested with 12 discrete input power levels – for better visibility, we indicated the full set of measurement points as individual dots only at a pump current of $I = 20\,\text{mA}$. The saturated output power for each pump current is found at an on-chip input power of 2.2 dBm, indicated by the respective measurement points. The horizontal dashed line indicates the saturation power $P_{sat}(100\,\text{mA}) = 11.4\,\text{dBm}$ at the RSOA facet.

To find the on-chip output power P_{out} of the ECL, we couple the light emitted from the Si$_3$N$_4$ output WG into an SMF. We then use the fiber-chip coupling loss, obtained from a straight reference WG on the same Si$_3$N$_4$ chip, to estimate the on-chip power levels P_{out}. In this experiment, we again tune the emission wavelength to approximately $\lambda = 1550\,\text{nm}$ and again vary the pump current between 20 mA and 100 mA in steps of 20 mA. For each current, we record the output spectrum using an OSA, and extract the peak powers $P_{out}(I)$. For an injection current of $I = 100\,\text{mA}$ an on-chip output power $P_{out}(100\,\text{mA}) = 9.6\,\text{dBm}$ is measured, see Fig. 4(b) for an exemplary ECL spectrum. Taking into account the attenuation of 0.1 dB of the resonance-aligned racetrack resonators and neglecting further on-chip losses, we find the output power $P_{out,PWB}(I)$ of the PWB. The PWB coupling efficiency is then estimated by taking the previously measured saturation RSOA output power $P_{sat}(I)$ as an input from the RSOA into the PWB in Fig. 1(b), $\eta_{PWB} = P_{out,PWB}(I)/P_{sat}(I)$. This leads to an estimated insertion loss of the PWB of $a_{PWB} = -10\log_{10}(\eta_{PWB}) = (1.6 \pm 0.2)\,\text{dB}$, see Fig. 4(c).

Fig. 4. Procedure for PWB loss estimation. We compare the on-chip output power P_{out} of the ECL to the saturated output power P_{sat} of the RSOA at the same wavelength $\lambda \approx 1550\,\text{nm}$ and the same injection currents I. **(a)** RSOA characterization results describing the current-dependent saturated output power $P_{\text{sat}}(I)$ of the RSOA. The data was obtained by launching light at a wavelength $\lambda \approx 1550\,\text{nm}$ into the RSOA through a circulator using an AR-coated lensed single-mode fiber (SMF) and by measuring the amplified signal after the circulator. We vary the RSOA pump current between 20 mA and 100 mA in steps of 20 mA and derive the associated relationships between the RSOA input and output power, both measured at the RSOA chip facet. The device was tested with 12 discrete input power levels – for better visibility, we indicated the full set of measurement points as individual dots only at a pump current of $I = 20\,\text{mA}$. The saturated output power for each pump current is found at an on-chip input power of 2.2 dBm, indicated by the respective measurement points. The horizontal dashed line indicates the saturation power $P_{\text{sat}}(100\,\text{mA}) = 11.4\,\text{dBm}$ at the RSOA facet. **(b)** Spectrum of the ECL emission when tuning the device to a wavelength of approximately $\lambda = 1550\,\text{nm}$. The injection current of $I = 100\,\text{mA}$ leads to an on-chip output power of $P_{\text{out}}(100\,\text{mA}) = 9.6\,\text{dBm}$. We again vary the pump current between 20 mA and 100 mA in steps of 20 mA and extract the peak powers $P_{\text{out}}(I)$ from the spectra measured by an OSA. **(c)** Result of PWB loss estimation for different RSOA injection currents. Taking into account the attenuation of 0.1 dB of the resonance-aligned racetrack resonators and neglecting further on-chip losses, we find the output power $P_{\text{out,PWB}}(I)$ of the PWB. The PWB coupling efficiency is then estimated by taking the previously measured saturation RSOA output power $P_{\text{sat}}(I)$ as an input from the RSOA into the PWB in Fig. 1(b), $\eta_{\text{PWB}} = P_{\text{out,PWB}}(I)/P_{\text{sat}}(I)$. This leads to an estimated insertion loss of the PWB of $a_{\text{PWB}} = -10\log_{10}(\eta_{\text{PWB}}) = (1.6 \pm 0.2)\,\text{dB}$.

Data availability. Data underlying the results presented in this paper are not publicly available at this time but may be obtained from the authors upon reasonable request.

References

1. Y. Xu, P. Maier, M. Blaicher, P.-I. Dietrich, P. Marin-Palomo, W. Hartmann, Y. Bao, H. Peng, M. R. Billah, S. Singer, U. Troppenz, M. Moehrle, S. Randel, W. Freude, and C. Koos, "Hybrid external-cavity lasers (ECL) using photonic wire bonds as coupling elements," Sci. Rep. **11**(1), (2021).
2. Y. Gao, J. Lo, S. Lee, R. Patel, L. Zhu, J. Nee, D. Tsou, R. Carney, and J. Sun, "High-power, narrow-linewidth, miniaturized silicon photonic tunable laser with accurate frequency control," J. Lightw. Technol. **38**(2), 265–271 (2020).
3. H. Guan, A. Novack, T. Galfsky, Y. Ma, S. Fathololoumi, A. Horth, T. N. Huynh, J. Roman, R. Shi, M. Caverley, Y. Liu, T. Baehr-Jones, K. Bergman, and M. Hochberg, "Widely-tunable, narrow-linewidth III-V/silicon hybrid external-cavity laser for coherent communication," Opt. Express **26**(7), 7920–7933 (2018).
4. M. A. Tran, D. Huang, J. Guo, T. Komljenovic, P. A. Morton, and J. E. Bowers, "Ring-resonator based widely-tunable narrow-linewidth Si/InP integrated lasers," IEEE J. Sel. Top. Quantum Electron. **26**(2), 1–14 (2020).
5. P. A. Morton, C. Xiang, J. B. Khurgin, C. D. Morton, M. Tran, J. Peters, J. Guo, M. J. Morton, and J. E. Bowers, "Integrated coherent tunable laser (ICTL) with ultra-wideband wavelength tuning and sub-100 Hz Lorentzian linewidth," J. Lightw. Technol. **40**(6), 1802–1809 (2022).
6. P. Pintus, J. Guo, W. Jin, M. A. Tran, J. Peters, C. Xiang, J. Liang, O. John, O. Iii, and J. E. Bowers, "225 GHz mode-hop-free tuning with a narrow linewidth integrated InP/Si laser," in *Conference on Lasers and Electro-Optics (CLEO)* (Optica Publishing Group, 2022), p. SM2P.3.
7. N. Kobayashi, K. Sato, M. Namiwaka, K. Yamamoto, S. Watanabe, T. Kita, H. Yamada, and H. Yamazaki, "Silicon photonic hybrid ring-filter external cavity wavelength tunable lasers," J. Lightw. Technol. **33**(6), 1241–1246 (2015).
8. R. Tang, T. Kita, and H. Yamada, "Narrow-spectral-linewidth silicon photonic wavelength-tunable laser with highly asymmetric Mach–Zehnder interferometer," Opt. Lett. **40**(7), 1504–1507 (2015).
9. K.-J. Boller, A. van Rees, Y. Fan, J. Mak, R. E. M. Lammerink, C. A. A. Franken, P. J. M. van der Slot, D. Marpaung, C. Fallnich, J. P. Epping, R. M. Oldenbeuving, D. Geskus, R. Dekker, I. Visscher, R. Grootjans, C. G. H. Roeloffzen, M. Hoekman, E. J. Klein, A. Leinse, and R. G. Heideman, "Hybrid integrated semiconductor lasers with silicon nitride feedback circuits," Photonics **7**(1), 4 (2019).
10. A. van Rees, Y. Fan, D. Geskus, E. J. Klein, R. M. Oldenbeuving, P. J. M. van der Slot, and K.-J. Boller, "Ring resonator enhanced mode-hop-free wavelength tuning of an integrated extended-cavity laser," Opt. Express **28**(4), 5669–5683 (2020).
11. Y. Guo, R. Zhao, G. Zhou, L. Lu, A. Stroganov, M. Nisar, J. Chen, and L. Zhou, "Thermally tuned high-performance III-V/Si₃N₄ external cavity laser," IEEE Photonics J. **13**(2), 1–13 (2021).
12. X. Li, Y. Guo, C. Liu, X. Li, M. Jin, E. Siyu, W. Xu, L. Lu, J. Chen, and L. Zhou, "FMCW source based on a hybrid integrated III-V/ Si-Si₃N₄ dual-layer external cavity laser," in *Conference on Lasers and Electro-Optics* (Optica Publishing Group, 2022), p. SM2P.7.
13. I. Ghannam, B. Shen, F. Merget, and J. Witzens, "Silicon nitride external cavity laser with alignment tolerant multi-mode RSOA-to-PIC interface," IEEE J. Sel. Top. Quantum Electron. **28**(1), 1–10 (2022).
14. Y. Fan, A. van Rees, P. J. M. van der Slot, J. Mak, R. M. Oldenbeuving, M. Hoekman, D. Geskus, C. G. H. Roeloffzen, and K.-J. Boller, "Hybrid integrated InP-Si₃N₄ diode laser with a 40-Hz intrinsic linewidth," Opt. Express **28**(15), 21713–21728 (2020).

15.   Y. Fan, J. P. Epping, R. M. Oldenbeuving, C. G. H. Roeloffzen, M. Hoekman, R. Dekker, R. G. Heideman, P. J. M. van der Slot, and K.-J. Boller, "Optically integrated InP–Si$_3$N$_4$ hybrid laser," IEEE Photonics J. **8**(6), 1–11 (2016).
16.   B. Stern, X. Ji, Y. Okawachi, A. L. Gaeta, and M. Lipson, "Battery-operated integrated frequency comb generator," Nature **562**(7727), 401–405 (2018).
17.   B. Kuyken, F. Leo, S. Clemmen, U. Dave, R. Van Laer, T. Ideguchi, H. Zhao, X. Liu, J. Safioui, S. Coen, S. P. Gorza, S. K. Selvaraja, S. Massar, R. M. Osgood, P. Verheyen, J. Van Campenhout, R. Baets, W. M. J. Green, and G. Roelkens, "Nonlinear optical interactions in silicon waveguides," Nanophotonics **6**(2), 377–392 (2017).
18.   Y. Vilenchik, C. T. Santis, S. T. Steger, N. Satyan, and A. Yariv, "Theory and observation on non-linear effects limiting the coherence properties of high-Q hybrid Si/III-V lasers," in *Novel In-Plane Semiconductor Lasers XIV* (SPIE, 2015), p. 93820N.
19.   D. Liang, A. W. Fang, H. Park, T. E. Reynolds, K. Warner, D. C. Oakley, and J. E. Bowers, "Low-temperature, strong SiO$_2$-SiO$_2$ covalent wafer bonding for III–V compound semiconductors-to-silicon photonic integrated circuits," J. Electron. Mater. **37**(10), 1552–1559 (2008).
20.   P. Maier, Y. Chen, Y. Xu, M. Blaicher, D. Geskus, R. Dekker, J. Liu, P.-I. Dietrich, H. Peng, S. Randel, W. Freude, T. J. Kippenberg, and C. Koos, "InP/Si$_3$N$_4$ hybrid external-cavity laser with sub-kHz linewidth acting as a pump source for Kerr frequency combs," in *European Conference on Optical Communication (ECOC)* (2022), p. We2E.4.
21.   M. Blaicher, M. R. Billah, J. Kemal, T. Hoose, P. Marin-Palomo, A. Hofmann, Y. Kutuvantavida, C. Kieninger, P.-I. Dietrich, M. Lauermann, S. Wolf, U. Troppenz, M. Moehrle, F. Merget, S. Skacel, J. Witzens, S. Randel, W. Freude, and C. Koos, "Hybrid multi-chip assembly of optical communication engines by in situ 3D nano-lithography," Light Sci. Appl. **9**(1), (2020).
22.   P.-I. Dietrich, M. Blaicher, I. Reuter, M. R. Billah, T. Hoose, A. Hofmann, C. Caer, R. Dangel, B. J. Offrein, U. Troppenz, M. Moehrle, W. Freude, and C. Koos, "In situ 3D nanoprinting of free-form coupling elements for hybrid photonic integration," Nat. Photonics **12**(4), 241–247 (2018).
23.   P. Maier, Y. Xu, M. Lauermann, A. Henniger-Ludwig, H. Kapim, M. Trappen, T. Kind, A. Weber, M. Blaicher, P.-I. Dietrich, C. Wurster, S. Randel, W. Freude, and C. Koos, "3D-printed optical elements for coupling of VCSEL and photodiode arrays to multi-core fibers in an SFP transceiver assembly," in *Optical Fiber Communication Conference (OFC)* (Optica Publishing Group, 2022), p. W2A.1.
24.   P. Maier, Y. Xu, M. Trappen, M. Lauermann, A. Henniger-Ludwig, H. Kapim, T. Kind, P. Dietrich, A. Weber, M. Blaicher, C. Wurster, S. Randel, W. Freude, and C. Koos, "3D-printed facet-attached optical elements for connecting VCSEL and photodiodes to fiber arrays and multi-core fibers," Opt. Express (accepted).
25.   D. Kharas, J. J. Plant, W. Loh, R. B. Swint, S. Bramhavar, C. Heidelberger, S. Yegnanarayanan, and P. W. Juodawlkis, "High-power (>300 mW) on-chip laser with passively aligned silicon-nitride waveguide DBR cavity," IEEE Photonics J. **12**(6), 1–12 (2020).
26.   C. Xiang, P. A. Morton, and J. E. Bowers, "Ultra-narrow linewidth laser based on a semiconductor gain chip and extended Si$_3$N$_4$ Bragg grating," Opt. Lett. **44**(15), 3825–3828 (2019).
27.   S. Watanabe, S. Takahashi, K. Suzuki, T. Takeuchi, Y. Deki, T. Hatanaka, N. Sakuma, A. Kawauchi, S. Takaesu, M. Horie, T. Miyazaki, M. Kurihara, M. Kanemoto, T. Kaneko, I. Tomita, M. Namiwaka, M. Nido, and H. Yamazaki, "High power tunable resonated-ring-reflector laser using passive alignment technology," in *European Conference on Optical Communications (ECOC)* (2006), pp. 1–2.
28.   M. H. P. Pfeiffer, A. Kordts, V. Brasch, M. Zervas, M. Geiselmann, J. D. Jost, and T. J. Kippenberg, "Photonic Damascene process for integrated high-Q microresonator based nonlinear photonics," Optica **3**(1), 20–25 (2016).
29.   H. Guo, M. Karpov, E. Lucas, A. Kordts, M. H. P. Pfeiffer, V. Brasch, G. Lihachev, V. E. Lobanov, M. L. Gorodetsky, and T. J. Kippenberg, "Universal dynamics and deterministic switching of dissipative Kerr solitons in optical microresonators," Nat. Phys. **13**(1), 94–102 (2016).
30.   P. Trocha, M. Karpov, D. Ganin, M. H. P. Pfeiffer, A. Kordts, S. Wolf, J. Krockenberger, P. Marin-Palomo, C. Weimann, S. Randel, W. Freude, T. J. Kippenberg, and C. Koos, "Ultrafast optical ranging using microresonator soliton frequency combs," Science **359**(6378), 887–891 (2018).
31.   J. Liu, H. Tian, E. Lucas, A. S. Raja, G. Lihachev, R. N. Wang, J. He, T. Liu, M. H. Anderson, W. Weng, S. A. Bhave, and T. J. Kippenberg, "Monolithic piezoelectric control of soliton microcombs," Nature **583**(7816), 385–390 (2020).
32.   J. Liu, A. S. Raja, M. Karpov, B. Ghadiani, M. H. P. Pfeiffer, B. Du, N. J. Engelsen, H. Guo, M. Zervas, and T. J. Kippenberg, "Ultralow-power chip-based soliton microcombs for photonic integration," Optica **5**(10), 1347–1353 (2018).
33.   A. S. Raja, A. S. Voloshin, H. Guo, S. E. Agafonova, J. Liu, A. S. Gorodnitskiy, M. Karpov, N. G. Pavlov, E. Lucas, R. R. Galiev, A. E. Shitikov, J. D. Jost, M. L. Gorodetsky, and T. J. Kippenberg, "Electrically pumped photonic integrated soliton microcomb," Nat. Commun. **10**, 680 (2019).
34.   B. Shen, L. Chang, J. Liu, H. Wang, Q.-F. Yang, C. Xiang, R. N. Wang, J. He, T. Liu, W. Xie, J. Guo, D. Kinghorn, L. Wu, Q.-X. Ji, T. J. Kippenberg, K. Vahala, and J. E. Bowers, "Integrated turnkey soliton microcombs," Nature **582**(7812), 365–369 (2020).
35.   T. C. Briles, S.-P. Yu, L. Chang, C. Xiang, J. Guo, D. Kinghorn, G. Moille, K. Srinivasan, J. E. Bowers, and S. B. Papp, "Hybrid InP and SiN integration of an octave-spanning frequency comb," APL Photonics **6**(026102), (2021).
36.   C. Xiang, J. Liu, J. Guo, L. Chang, R. N. Wang, W. Weng, J. Peters, W. Xie, Z. Zhang, J. Riemensberger, J. Selvidge, T. J. Kippenberg, and J. E. Bowers, "Laser soliton microcombs heterogeneously integrated on silicon," Science **373**(6550), 99–103 (2021).
37.   W. Jin, Q.-F. Yang, L. Chang, B. Shen, H. Wang, M. A. Leal, L. Wu, M. Gao, A. Feshali, M. Paniccia, K. J. Vahala, and J. E. Bowers, "Hertz-linewidth semiconductor lasers using CMOS-ready ultra-high-Q microresonators," Nat. Photonics **15**(5), 346–353 (2021).
38.   A. S. Voloshin, N. M. Kondratiev, G. V. Lihachev, J. Liu, V. E. Lobanov, N. Y. Dmitriev, W. Weng, T. J. Kippenberg, and I. A. Bilenko, "Dynamics of soliton self-injection locking in optical microresonators," Nat. Commun. **12**(235), (2021).